PASJ: Publ. Astron. Soc. Japan **46**, 527–538 and Plate 16–17 (1994)

Distribution and Dynamics of Molecular Gas in the Galaxy M51. I. Data and Spiral Structure

Naomasa NAKAI and Nario KUNO
*Nobeyama Radio Observatory,**
Minamimaki-mura, Minamisaku-gun, Nagano 384-13
E-mail (NN) nakai@nro.nao.ac.jp
and
Toshihiro HANDA and Yoshiaki SOFUE
Institute of Astronomy, The University of Tokyo, Mitaka, Tokyo 181

(Received 1994 January 21; accepted 1994 August 22)

Abstract

The ^{12}CO(J=1–0) line emission from the region of $6' \times 6'$ (17 kpc × 17 kpc) of M51 has been mapped with the Nobeyama 45-m telescope. The mapping area covers most of the optical disk. The spiral arms are clearly separated, and the CO emission from the interarm regions is well detected with high sensitivity. Two molecular arms are fitted by symmetrical logarithmic spirals at $40'' < R < 120''$, but are distorted at $R > 120''$ by the tidal interaction with the companion galaxy NGC 5195, where R is the galactocentric distance. The width of the molecular arms is 900–1000 pc and its displacement from Hα arms is 440 pc. The CO(2–1) to CO(1–0) intensity ratio is constant at 0.80 throughout the disk, except for the extreme outer region, and is almost the same as those previously measured in disks of other galaxies.

Key words: Galaxies: individual (M51) — Galaxies: ISM — Galaxies: spiral — Interstellar: molecules

1. Introduction

Carbon monoxide observations of galactic disks provide a crucial key for understanding the formation mechanism of stars and molecular clouds in spiral arms and interarms, as well as for investigating the structure and dynamics of the molecular arms. For these purposes the following observational conditions are required: (1) A spatial resolution better than one kpc in order to distinguish spiral arms and interarms, because the separation between arms is a few kpc. One kpc corresponds to 21″ at the distance of M51. (2) High sensitivity in order to detect the weak emission from interarm regions. (3) Large-field mapping to obtain statistically meaningful results, because arms and interarms are not uniform in CO and other emissions. (4) Mapping with a filled-aperture telescope which is sensitive even to the diffuse component of the molecular gas. Although numerous CO observations of external galaxies have been made for the past 15 yr, few observations have satisfied these conditions. We therefore mapped the ^{12}CO(J=1–0) emission in the entire disk of the grand-design spiral galaxy, M51, with the NRO 45-m telescope. With the high spatial resolution of HPBW= 16″ (745 pc) the spiral structure has been resolved and with the high sensitivity the CO emission from the interarm regions has been detected.

The galaxy M51 (NGC 5194, UGC 8493, Arp 85) is a nearby almost face-on galaxy with two clear spiral arms. Since the CO emission from the disk is relatively strong, it is easily detected. Although the galaxy is interacting with the companion galaxy NGC 5195, only the outer region of the disk is disturbed by the tidal force; the inner disk within a radius of 120″ is less affected, as shown in subsection 3.3. Thus, M51 is one of the most suitable galaxies for the above-mentioned purposes. The morphological type of M51 is SAbc (de Vaucouleurs et al. 1991) or Sbc I–II (Sandage, Tammann 1981). The distance to the galaxy has been reported to be 7.6 Mpc (de Vaucouleurs 1979), 8.7 Mpc (Aaronson, Mould 1983), 9.6 Mpc (Sandage, Tammann 1974), and 9.7 Mpc (Sandage, Tammann 1975). Throughout this paper we adopt 9.6 Mpc, following other literature. The nucleus of M51 is an AGN, as described in subsection 3.2, and shows an unresolved peak in the radio continuum emission (Ford et al. 1985; Crane, van der Hulst 1992); we thus define the continuum peak as the nucleus of the galaxy. The adopted parameters of M51 are summarized in table 1.

The CO emission in M51 has been mapped using various single-dish telescopes (NRAO 11 m: Rickard, Palmer 1981; FCRAO 14 m: Scoville, Young 1983, Lord, Young

* NRO is a branch of the National Astronomical Observatory, an inter-university research institute operated by the Ministry of Education, Science and Culture.

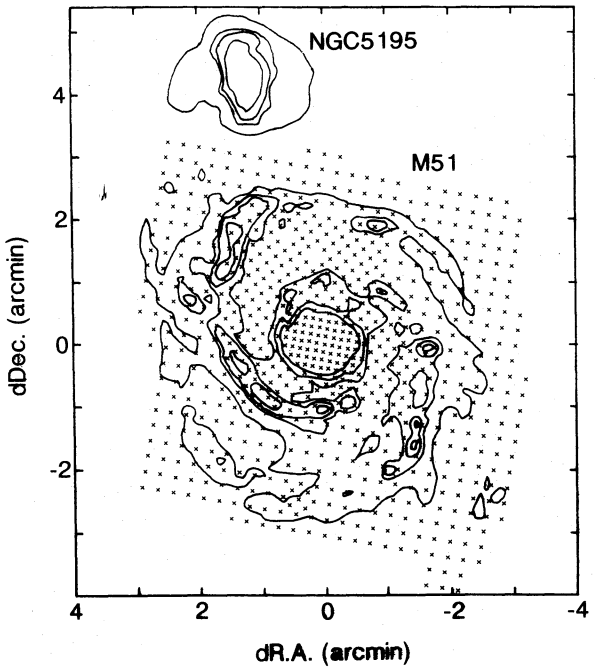

Fig. 1. Observing points (crosses) superposed on the isophotal contour map in the blue band (arbitrary unit). The grid points are spaced by 7.″5 in the inner disk and by 15″ in the outer disk parallel to the major and minor axes with the position angle of −10°. The top is north.

1990; Onsala 20 m: Rydbeck et al. 1985; IRAM 30 m: Garcia-Burillo et al. 1993a; Garcia-Burillo et al. 1993b) and interferometers (OVMI: Lo et al. 1987; Vogel et al. 1988; Rand, Kulkarni 1990; BIMA: Adler et al. 1992; NMA: Tosaki et al. 1994). Rand, Kulkarni (1990) presented an interferometric image covering most of the optical disk, and showed a narrow molecular spiral structure and giant molecular associations. Although such aperture-synthesis observations have provided a higher spatial resolution and a better positional accuracy, the interarm emission has hardly been visible. On the other hand, observations with large filled-aperture telescopes are sensitive even to the extended component and to weak emissions from the interarm regions. In this paper we present our data of ^{12}CO(1–0) observations with the NRO 45-m telescope and report on the results. Preliminary results of this survey have been reported by Nakai et al. (1990) and Kuno et al. (1990). Detailed discussions concerning the relation between molecular gas and star formation and the kinematical structure of molecular gas will be presented in forthcoming papers (Paper II and III).

Table 1. Parameters of M51.

Center position (1950.0)[1]	R.A. = $13^h27^m46.^s327$
	Decl. = 47°27′10.″25
Morphological type[2],[3]	Sbc
Systemic velocity (LSR)[4]	470 km s^{-1}
Distance[5]	9.6 Mpc
Position angle of major axis[6]	−10° ± 3°
Inclination angle(6)	20° ± 5°(90° is edge-on)
Beam size on galaxy (16″)	745 pc

(1) Position of 1.4 GHz radio continuum peak (Ford et al. 1985). (2) de Vaucouleurs et al. 1991. (3) Sandage and Tammann 1981. (4) Goad et al. (1979) and references therein. Corresponding heliocentric velocity is 462 km s^{-1}. (5) Sandage and Tammann 1974. (6) Tully 1974b.

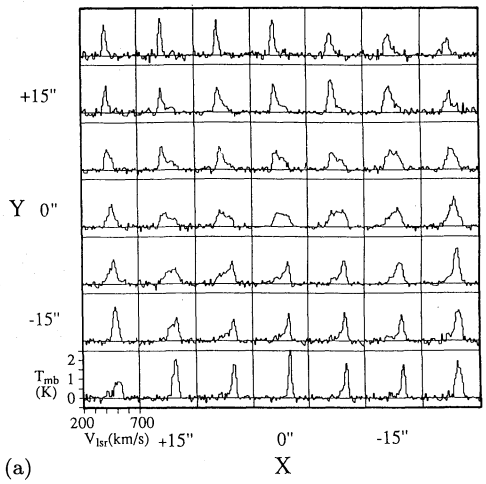

Fig. 2. (a) Measured spectra of ^{12}CO(1–0) emission in the central region of 45″ × 45″ parallel to the minor (X) and major (Y) axes. For each spectrum the abscissa is the LSR velocity (200–700 km s^{-1}) and the ordinate is the main-beam brightness temperature (−0.5–2.5 K). (b) Same as figure (a) but for all spectra.

2. Observations

Observations of the ^{12}CO(J=1–0) emission were made between 1986 and 1991 with the 45-m telescope of the Nobeyama Radio Observatory. The antenna is of Cassegrain design, with a single feed horn sensitive to one linear polarization. A quasi-optical system, which lays in front of the feed horn, contained a Martin-Puplett type SSB filter for an image sideband termination at the cryogenic temperature (4 K). At the 115.271204 GHz rest frequency of the ^{12}CO(J=1–0) transition, the full half-power beam width (HPBW) was 16″, which corresponds

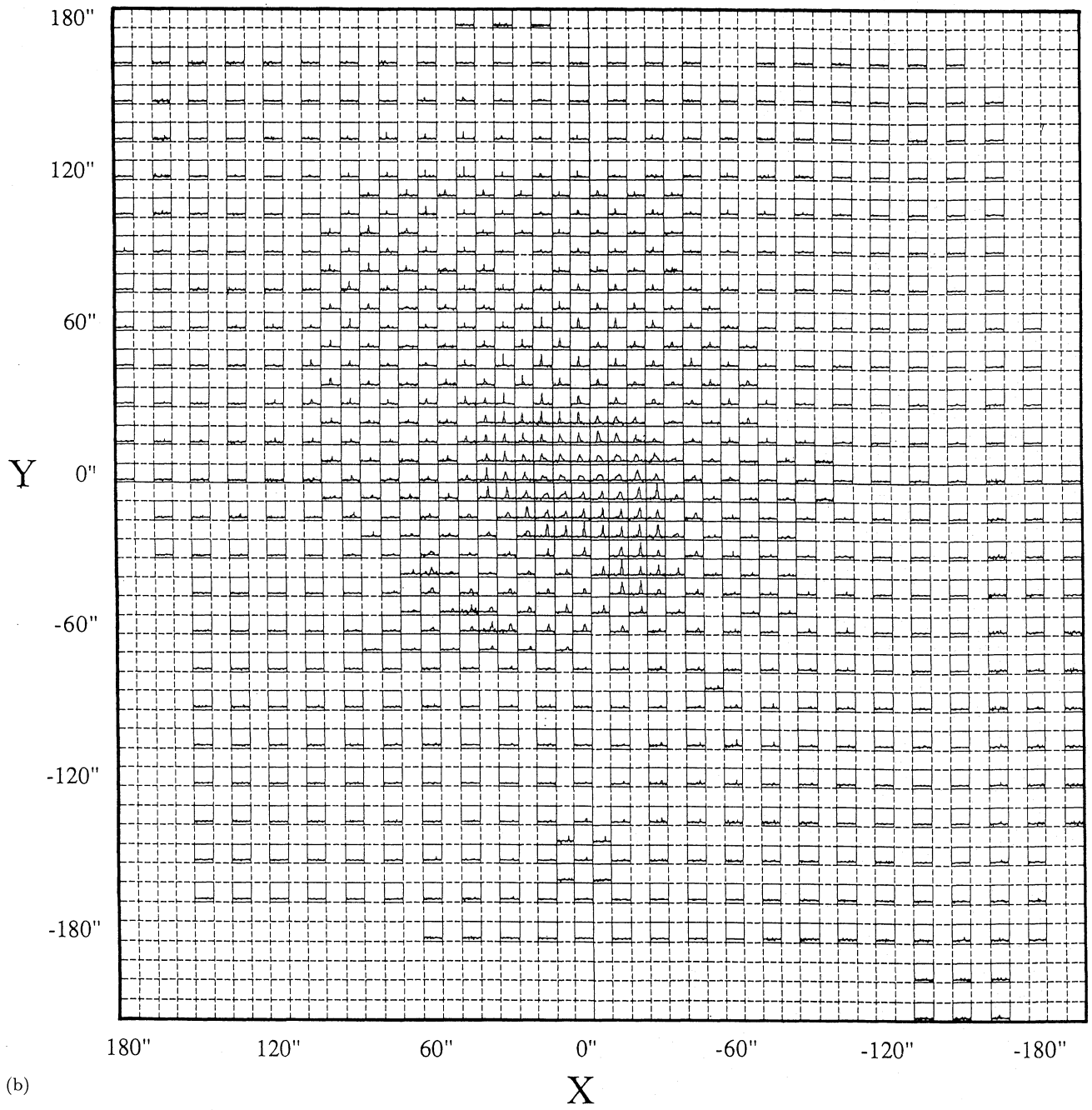

Fig. 2. (continued)

to 745 pc at a distance of 9.6 Mpc. The aperture and main-beam efficiencies were changed to be $\eta_a = 0.25$ to 0.36 and $\eta_{mb} = 0.35$ to 0.50 during the observing periods, though the data have been re-scaled to have $\eta_a = 0.36$ and $\eta_{mb} = 0.50$ (see below). These efficiencies were measured using the planets, Mars, Jupiter, and Saturn, whose brightness temperatures at 115 GHz were adopted to be 210 K, 180 K, and 150 K, respectively. The telescope efficiency was $\eta_l = 0.90$.

The receiver frontends used cooled Schottky-diode (1986–1990) and SIS (1991) mixers. The system noise temperature (SSB), including the atmospheric effect and the antenna ohmic loss, was 500–1200 K at the observing elevations. The receiver backends were the 2048-channel wide-band acousto-optical spectrometer (AOS). The frequency resolution and channel spacing were 250 kHz and

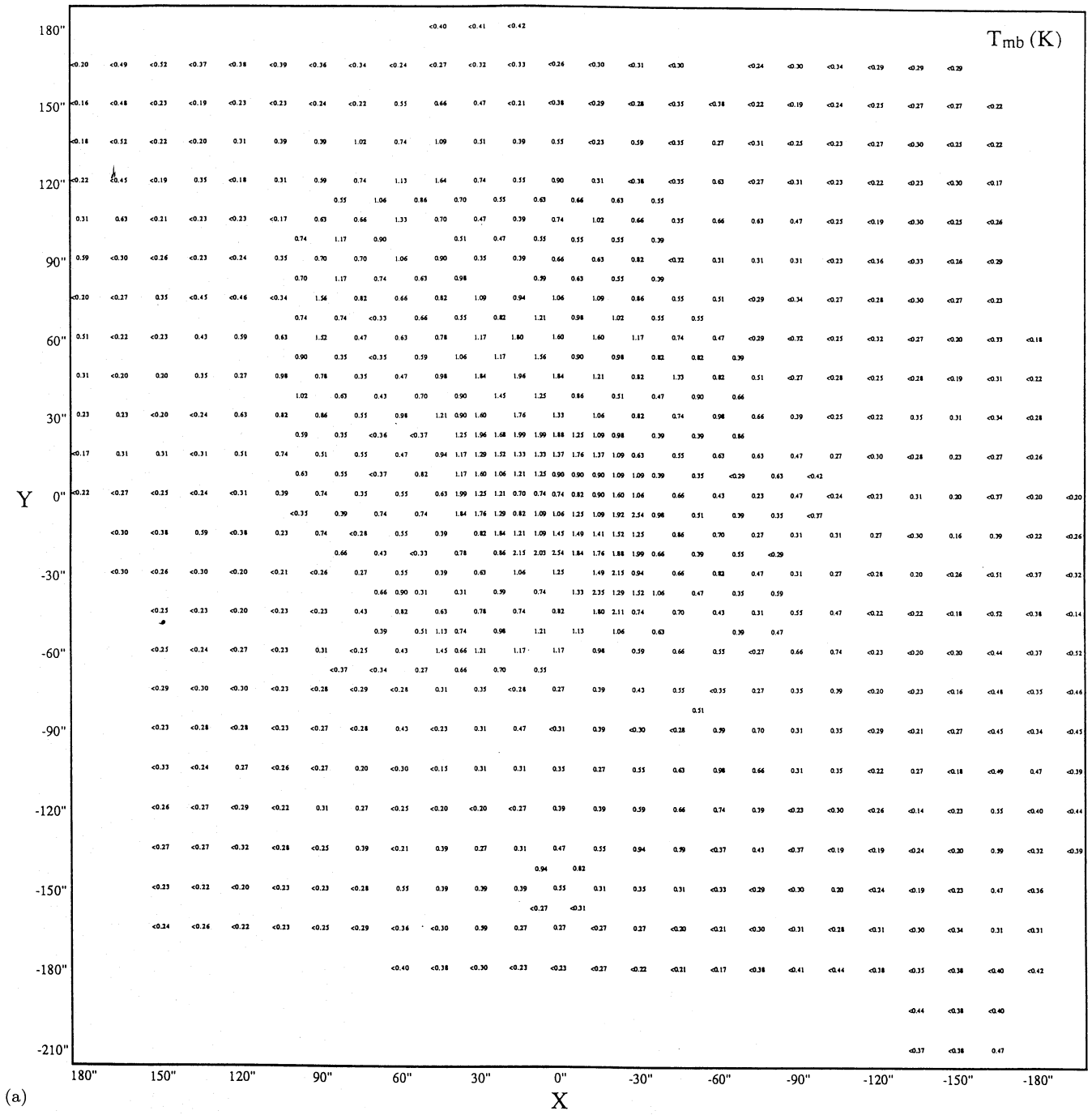

(a)

Fig. 3. (a) Peak main-beam brightness temperature, $T_{\rm MB}$, in K at all observing points. The coordinates X and Y are the offsets from the galactic center along the minor and major axes, respectively. The upper limits are $2\Delta T_{\rm rms}$. (b) Integrate intensity, $I_{\rm CO} \equiv \int T_{\rm MB} dv$, in K km s^{-1} at observing points. Dots indicates that no significant emission has been detected at the points. The rms noise is given by equation (1).

125 kHz, respectively, providing 250 MHz of the total bandwidth of an AOS. At 115 GHz the corresponding velocity resolution and velocity coverage were 0.65 km s^{-1} and 650 km s^{-1}, respectively.

The observations were made in the position-switching mode with six ON positions and two OFF positions at offsets of $\pm 7'$ from the galaxy center in azimuth. We observed all points in two to five separate series of runs

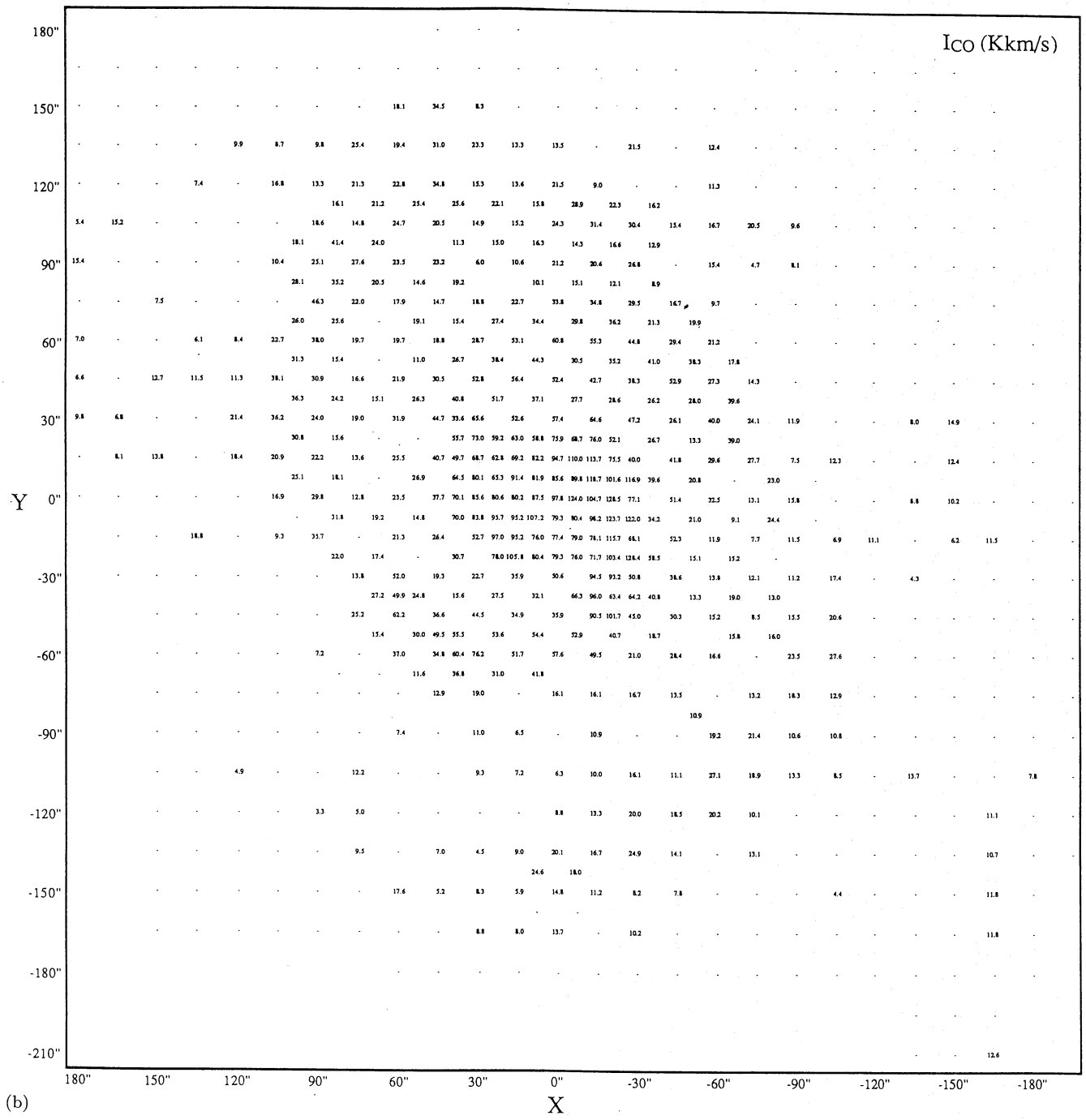

Fig. 3. (continued)

in order to decrease the effective pointing and intensity errors, and added them after the observations. The total integration time per point was typically 10 min. The telescope pointing was checked and calibrated every hour by observing the continuum emission of a QSO (RA_{1950} = $14^h18^m6^s.18$, $Decl_{1950}$ = $54°36'58''.05$), the HCN emission of a late-type star Y CVn ($RA_{1950} = 12^h42^m47^s.084$, $Decl_{1950}$ = $45°42'47''.88$), and the SiO maser emission of a late-type star R CVn (RA_{1950} = $13^h46^m48^s.56$, $Decl_{1950} = 39°47'26''.4$). These pointing calibrators were observed with the 40-GHz band receiver; the pointing difference between the 40-GHz and 100-GHz band receivers was less than $1''$. The absolute pointing accuracy was better than $\pm 4''$ (peak value) throughout the observa-

tions.

The calibration of the line intensity was made using an absorbing chopper wheel in front of the receivers, which yielded the antenna temperature T_A^* corrected for the atmospheric and antenna ohmic losses. The probable error of T_A^* was within $\pm 20\%$. In this paper we use as the intensity scale the main-beam brightness temperature, defined by $T_{MB} \equiv T_A^*/\eta_{mb}$. Since we used two receivers and the antenna gain changed during the observations, the measured CO intensity may not have been constant, even on the scale of the brightness temperature. In order to avoid this intensity variation, we scaled T_{MB} at each point by observing some reference points. The corresponding η_{mb} is 0.50 for all spectra.

We observed 768 points in the region of about $6' \times 6'$ (≈ 17 kpc $\times 17$ kpc), which contains most of the optical disk, with the map center at the 1.4 GHz radio continuum peak. CO spectra were sampled at grid points spaced by $7''.5$ (350 pc) in the inner region and by $15''$ (700 pc) in the outer region parallel to the major and minor axes with a position angle of $-10°$. Figure 1 shows the observing positions superposed on the isophotal contour map in the blue band.

3. Data and Results

3.1. Spectra

Figures 2a and 2b show the measured spectra of ^{12}CO(1–0) emission in the central $45'' \times 45''$ region and in the whole disk, respectively, where the spectra have been smoothed to a velocity resolution of 5 km s^{-1}. In both figures, the velocity range is 200 km s^{-1} to 700 km s^{-1} in the LSR velocity, V_{LSR} ($= V_{hel} + 8$ km s^{-1}), and the temperature range -0.5 K to 2.5 K in T_{MB}. The X- and Y-coordinates originate at the galactic center and are parallel to the minor and major axes, respectively.

Figures 3a and 3b show the values of the peak main-beam brightness temperature T_{MB} in K, and the integrated intensity $I_{CO} \equiv \int T_{MB} dv$ in K km s^{-1} of all spectra. Figure 3a includes upper limits represented by 2σ levels ($2\Delta T_{rms}$), while figure 3b does not present values at points where no significant emission was detected (denoted by dots). One σ of I_{CO} for a typical velocity width ($\Delta V_i \approx 20$ km s^{-1}) in the disk is given by

$$\Delta I_{rms} = \Delta T_{rms} \Delta V_i (\Delta V_s/\Delta V_i)^{1/2} = 10 \Delta T_{rms} (\Delta V_i/20 \text{ km s}^{-1})^{1/2} \text{ K km s}^{-1}, \quad (1)$$

where ΔV_s is the smoothed channel width (5 km s^{-1}) and ΔT_{rms} can be obtained as half values in figure 3a. The conversion of coordinates from (X,Y) to $(\Delta RA, \Delta Decl)$ is given by

$$\Delta RA = 0.9848X - 0.1736Y, \quad \Delta Decl = 0.1736X + 0.9848Y. \quad (2)$$

The brightness temperature on the spiral arms is found to be ≥ 0.5–1 K, while the temperature in the interarm regions is typically ≈ 0.3 K. The line width of the CO spectra is typically $\Delta V_{FWHM} \approx 20$ km s^{-1} in the disk. The width was observed to be as large as 200 km s^{-1} at the central region, where the rotation curve of the galaxy is unresolved, and the broad line width is mainly due to a coupling of the telescope beam and the sharply rising rotation curve. A detailed analysis of the velocity field and the line width will be given in Paper III. No line emission with peculiar velocities far from the galactic rotation (like high velocity clouds in our Galaxy) has been detected within the noise level. The upper limit (2σ) of the H_2 column density for such "high-velocity gas" is estimated to be $\approx 6 \times 10^{20}$ H_2 cm^{-2} for $\Delta T_{rms} \approx 0.1$ K and assumed $\Delta V \approx 20$ km s^{-1}, using equation (1) and the conversion factor of $N(H_2)/I_{CO} = 3 \times 10^{20}$ H_2 cm^{-2} evaluated for low I_{CO} in M51 (Nakai, Kuno 1994)

3.2. CO Distribution in the Central Region

The distributions of I_{CO} and peak T_{MB} in the central $100'' \times 100''$ region are shown in figures 4a and 4b, respectively. A strong I_{CO} has been obtained within $R \approx 40''$; the distribution has a bar-like elongation with a semi-major axis of $\approx 25''$ and a position angle of $\approx 110°$. The nonaxisymmetric structure is also seen in CO maps of Rand and Kulkarni (1990), Garcia-Burillo et al. (1993b), and Tosaki et al. (1994), where the position angle of the elongation is 130°–140°. The length and the position angle are close to those of an oval structure in the near-infrared (I, J, H, and K) images ($R \approx 20''$, $P.A. \approx 135°$: Pierce 1986; Thronson, Greenhouse 1988). Since the near-infrared images indicate the distribution of the stellar mass density, the bar-like elongation of the CO distribution could be due to an elliptical orbit of molecular clouds caused by a nonaxisymmetric gravitational potential like that in a barred galaxy.

Regions with the most intense I_{CO} are located around the ends of the bar/oval, from which two spiral arms emerge toward the north and south, and comprise an insufficient ring-like structure, which can be more clearly seen in figure 4b, although the deep central hole in the figure is mainly due to the velocity dilution. The radius of the ring is $25'' \pm 5''$ ($= 1.2$ kpc ± 0.2 kpc). Similar ring-like structures at the same radius are seen in Hα (Tully 1974a; van der Hulst et al. 1988), far-infrared (Lester et al. 1986), and very blue color of $B - V < 0^m.2$ (Worden 1974) and $B - I \sim 0^m.9$ (Pierce 1986), indicating the active formation of massive stars in the ring.

The nucleus of M51 shows characteristics of LINERs or Seyferts: The ratio of [N II]/Hα at and around the nucleus is 2–7, indicating a non-thermal nuclear source of ionizing photons or shock heating, and both emission lines have very broad wings of ≤ 1800 km s^{-1} (Burbidge,

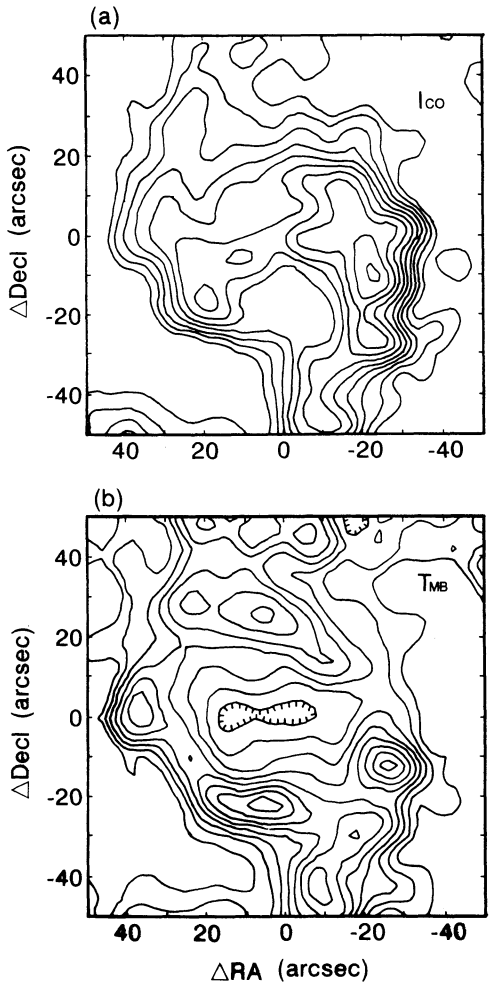

Fig. 4. (a) Contour map of the integrated intensity (I_{CO}) in the central $100'' \times 100''$ region. The first contour and contour interval are 45 and 9 K km s^{-1}, respectively. (b) Contour map of the peak brightness temperature (T_{MB}) in the same region as (a). The first contour and contour interval are 0.8 K and 0.2 K, respectively.

Burbidge 1964; Goad et al. 1979; Rose, Searle 1982; Rose, Cecil 1983; Cecil, Rose 1984; Goad, Gallagher 1985; Hua et al. 1987; Cecil 1988). The hard X-ray spectrum shows emission from a weak Seyfert nucleus (Makishima et al. 1990). Radio continuum observations at 20 cm and 6 cm have revealed bubbles/jets emanating from the nucleus toward the north-south directions (Ford et al. 1985; Crane, van der Hulst 1992). High-velocity components of Hα and [H II] also show a bubble-like structure (Cecil 1988). These results strongly suggest that the ionized gas and a relativistic plasma are ejected from the active nucleus. The appearance of the jets is clearly bipolar, in spite of the nearly face-on view of the galactic disk, extending by $14''$ and $6''$ (650 pc and 280 pc) toward the north and south, respectively, at almost the same position angle as the major axis of the galactic disk. Therefore, the direction of the outflow is not perpendicular to the disk, but is tilted (Ford et al. 1985; Cecil 1988). In this case, it is expected that the nuclear outflow interacts with the gas around the nucleus, as seen in the central region of NGC 1068 (Kaneko et al. 1989). However, the spectra (figure 2) and distribution of I_{CO} (figure 4a) of CO do not show any feature suggestive of such an interaction with the outflow within the noise level.

3.3. *Structure of Molecular Arms*

Figure 5 shows a contour map of I_{CO} for the entire disk of M51, and figure 6 (Plate 16) gives its colour image. Two spiral arms can be clearly seen. The width (FWHM) of the CO arms corrected for the telescope beam width is measured to be 900–1000 pc, and is nearly constant along the arms, except for $R < 60''$, where the spacing between two arms is not much broader than the beam size. The arm width of ~ 1 kpc is consistent with those of the CO(1–0) arms obtained by combining the BIMA data with the Onsala 20m-telescope data (Adler et al. 1992) and of the CO(2–1) arms measured with the IRAM 30-m (Garcia-Burillo et al. 1993b). Local maxima of the CO intensity are aligned along the arms with a nearly constant spacing of 1.6 ± 0.3 kpc within $R \approx 90''$ where the observed points are fully sampled with a spacing of half beam size (figure 1). This result will be discussed in Paper II in relation to the Parker instability (but also see Verschuur 1993).

The angle between a spiral arm and the azimuthal direction, i.e., the pitch angle p is given by

$$\frac{1}{R}\frac{dR}{d\theta} = \tan p, \tag{3}$$

where R and θ are the distance from the center and the azimuthal angle of an arm for a face-on view, respectively. If p is a constant, equation (3) can be integrated, giving

$$\theta = \frac{1}{\tan p} \ln\left(\frac{R}{R_0}\right) + \theta_0, \tag{4}$$

or

$$R = k \exp(\theta \tan p), \tag{5}$$

where R_0 and θ_0 are constants and $k = R_0 \exp(-\theta_0 \tan p)$. Equation (4) indicates that a spiral arm is traced by a straight line in a ($\ln R$, θ) plane, which is called a logarithmic spiral. Figure 7 is a $\ln R$–θ plot of I_{CO}, where θ is measured counterclockwise from $P.A. = -10°$ and the inclination angle ($i = 20°$; Tully 1974b) is corrected. Both of the two CO arms can be fitted by straight lines at $40'' \leq R \leq 120''$ (1.9 kpc $\leq R \leq$ 5.5 kpc), with a pitch angle of $p = 21° \pm 5°$, which is consistent with the value optically determined ($18.°5 \pm 0.°5$; Tully 1974c). However, the logarithmic spirals are broken at

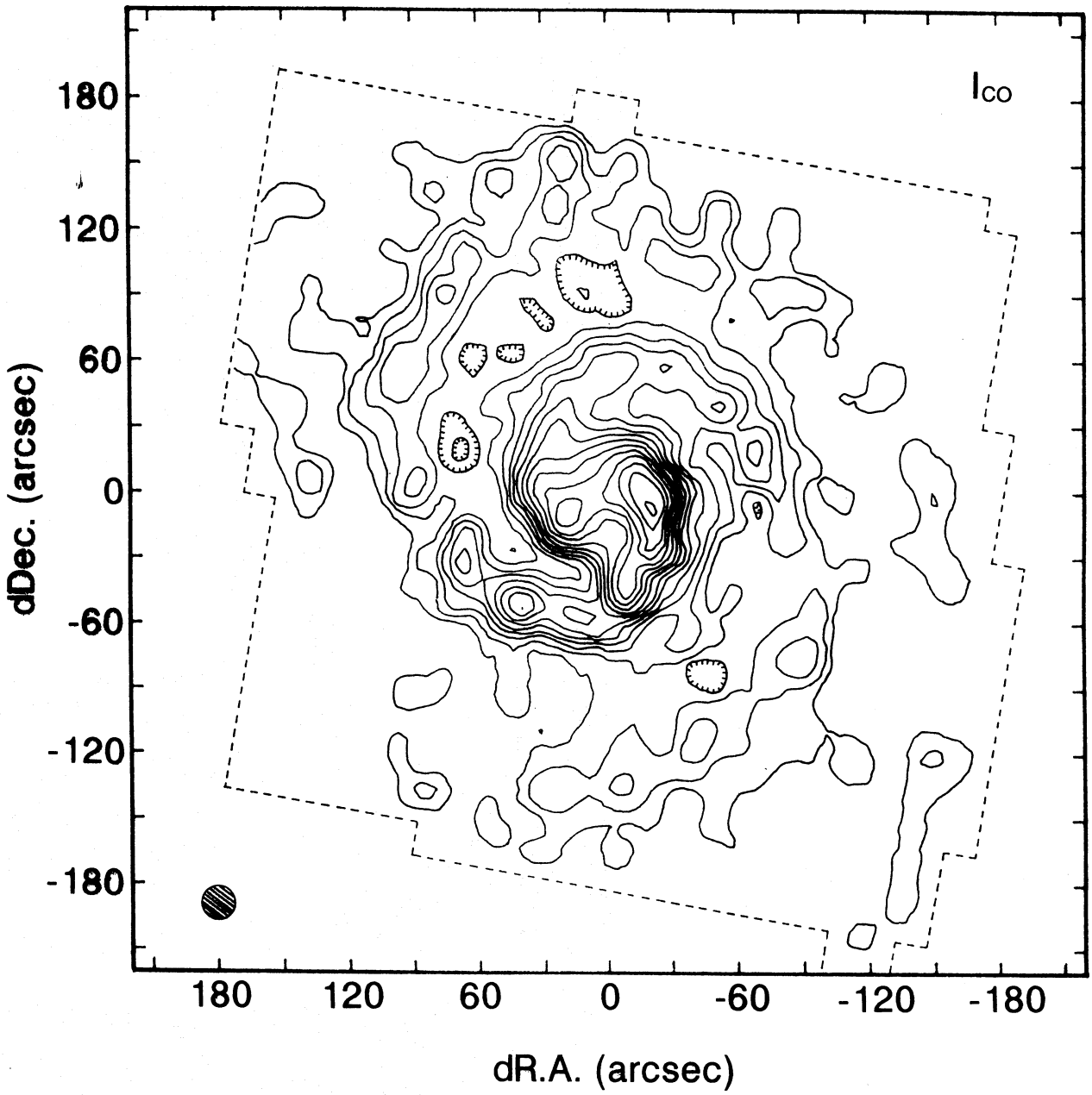

Fig. 5. Contour map of the CO integrated intensity for all data. The mapping area is represented by dotted lines. The first contour and contour interval are 8 K km s^{-1}. The HPBW of the telescope is denoted by a hatched circle.

$R \approx$ 5.5–6.0 kpc and $\theta \approx$ 52°–67° and −122°––134° (*P.A.* ≈ 42°–57° and −132°––144°). Such fractures of the spiral arms have also been pointed out in Hα images (Tully 1974c). This distortion can be caused by a tidal interaction with the companion galaxy, NGC 5195. Non-self-gravitating (Toomre, Toomre 1972; Toomre 1981) and self-gravitating (Byrd, Howard 1990) simulations of the M51/NGC 5195 system show that although the outer disk of M51 is disturbed by NGC 5195, the inner disk keeps its original shape. Our CO observations are in a good agreement with these particle simulations.

Figure 8 (Plate 17) shows an overlay of the contour map of I_{CO} on an optical image of Sandage and Bedke (1988). The molecular arms are strongly correlated with dark lanes, and bright optical ridges are distributed outside the molecular arms. This trend is also shown in figure 9: Ridges of the CO intensity (solid lines) are offset from those of Hα (dotted lines), generally toward the inside. The mean value of the offset is 440 pc ± 370 pc ($9'' \pm 8''$). The separation between the CO and Hα arms

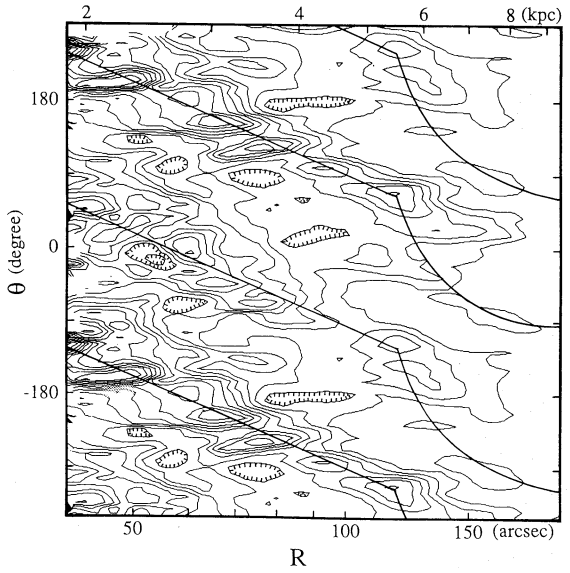

Fig. 7. ln R–θ plot of the integrated intensity (I_{CO}) at $40'' \leq R \leq 200''$, where θ is measured counterclockwise from $P.A. = -10°$ and the inclination angle (20°) has been corrected. At $R < 40''$, observing points are not enough to draw contours and no arm appears. Both the CO arms can be fitted by logarithmic spirals at $40'' \leq R \leq 120''$ (straight line) but are distorted at $R > 120''$ (curved lines).

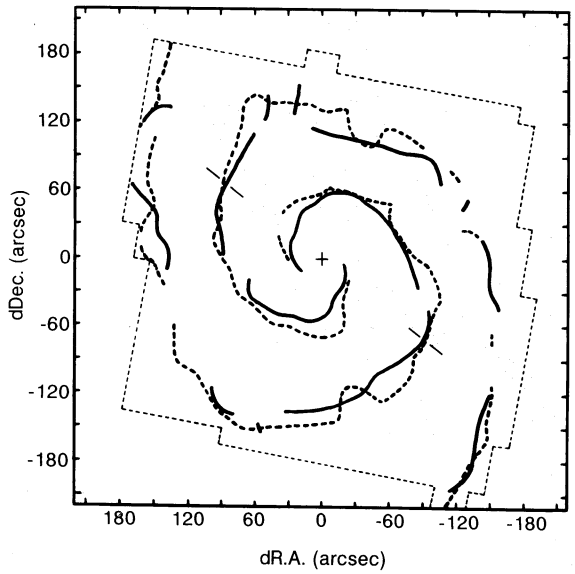

Fig. 9. Loci of the intensity peaks of CO (solid lines) and Hα (dotted lines: van der Hulst et al. 1988). Positions of the fractures of the CO spiral arms are denoted by thin lines at $P.A. \approx 50°$ and 230°. A cross indicates the center of M51 and thin dotted lines show the CO mapping area.

continues even along the outer arms over the above fracture points ($P.A. \approx 50°$ and 230°), indicating that density waves exist even along the outer arms. The positional relation is, however, unclear in the extreme outer parts of the arms at $R \geq 7$ kpc and $P.A. \leq -50°$ or 160°, because the CO emission is weak and the CO observing points are sparse ($15'' \approx$ HPBW). The offset of the CO arms from the Hα arms in M51 has been also noted by Vogel et al. (1988), Rand and Kulkarni (1990), and Garcia-Burillo et al. (1993b). Although a part of this offset could be due to optical extinction, we note that almost the same offset value ($\approx 10'' \approx 470$ pc) has been observed between the nonthermal radio continuum emission, which coincides with dust lanes, and the thermal radio continuum emission, which coincides with Hα emissions (Tilanus et al. 1988).

3.4. *Ratio of CO(2–1) to CO(1–0) Line Intensities*

The ratio of ^{12}CO(2–1) to ^{12}CO(1–0) line intensities helps to constrain the physical state of the CO gas. Figure 10a shows the ratio of the integrated intensity between the two transitions, $R_{21} \equiv I_{CO}(2\text{–}1)/I_{CO}(1\text{–}0)$, where $I_{CO}(2\text{–}1)$ ($\equiv \int T_A^* dv/\eta_{mb}$, $\eta_{mb} = 0.46$) was adopted from the map obtained with the IRAM 30-m telescope(Garcia-Burillo et al. 1993b). The difference of beam sizes [HPBW = $16''$ for CO(1–0) and $12''$ for CO(2–1)] was not corrected. The R_{21} was calculated at observing points within a radius of $150''$, where both the CO(1–0) and CO(2–1) emissions were detected . Figure 10a indicates that the R_{21} is almost constant (0.78 ± 0.27) at $R < 120''$ and slightly larger (1.05 ± 0.43) at $R > 120''$. The mean R_{21} over the whole disk ($R < 150''$) is 0.80 ± 0.30, which is consistent with the value (0.8) obtained by Garcia-Burillo et al. (1993b).

If we assume the same line widths for the two transitions and $T_{MB} \approx T_R$ (= radiation temperature), $R_{21} = I_{CO}(2\text{–}1)/I_{CO}(1\text{–}0) \approx T_{MB}(2\text{–}1)/T_{MB}(1\text{–}0) \approx T_R(2\text{–}1)/T_R(1\text{–}0)$. The radiation transfer equation gives the temperature ratio,

$$\frac{T_R(2\text{–}1)}{T_R(1\text{–}0)} = \frac{f(2\text{–}1)[J_\nu\{T_{ex}(2\text{–}1)\} - J_\nu\{T_{bg}\}]\{1 - \exp(-\tau_{21})\}}{f(1\text{–}0)[J_\nu\{T_{ex}(1\text{–}0)\} - J_\nu\{T_{bg}\}]\{1 - \exp(-\tau_{10})\}}, \quad (6)$$

where J_ν is the Planck function,

$$J_\nu = (h\nu/k)\{\exp(h\nu/kT_{ex} - 1\}^{-1}, \quad (7)$$

f the filling factor, T_{ex} the excitation temperature, T_{bg} the background radiation temperature, τ the optical depth, h Planck's constant, k Boltzman's constant, and ν the frequency. The ratio of the optical depth between the two transitions is

$$\frac{\tau_{21}}{\tau_{10}} = 2\frac{1 - \exp\{-h\nu_{21}/kT_{ex}(2\text{–}1)\}}{\exp\{h\nu_{10}/kT_{ex}(1\text{–}0)\} - 1}, \quad (8)$$

Table 2. Reduced parameters for the molecular arms.

Width (FWHM)*	900–1000 pc
Pitch angle†	21° ± 5°
Displacement from Hα arms	440 pc ± 370 pc
Distance of the fracture points	120″–130″
from the center	(5.5–6.0 kpc)

* Corrected for telescope beam width.
† at $40'' \leq R \leq 120''$ (1.9 kpc $\leq R \leq$ 5.5 kpc).

where ν_{21} and ν_{10} are the frequencies of the ^{12}CO(2–1) and ^{12}CO(1–0) lines, respectively. From equations (6) and (8) and the assumptions of f(1–0) $\approx f$(2–1) and T_{ex}(1–0) $\approx T_{ex}$(2–1), the observed value of R_{21} [$\approx T_R$(2–1)/T_R(1–0)] $\approx$ 0.8 in figure 10a indicates large optical depths (τ_{10}, $\tau_{21} \gg 1$) with $T_{ex} \geq 7$ K. Although there is a possibility of optically thin ($\tau \ll 1$) for very low excitation temperature ($T_{ex} \approx$ 5–6 K) for the R_{21} ratio, such a physical state is excluded by the ^{12}CO/^{13}CO ratio: Rickard and Blitz (1985) and Young and Sanders (1986) obtained the ^{12}CO(1–0)/^{13}CO(1–0) intensity ratio of 5.4–8.4 and 12.4 ± 2.4 in the disk of M51, respectively. These values are much smaller than the cosmic abundance of [^{12}C]/[^{13}C] $\approx$ 90 and strongly suggests optically thick emission of ^{12}CO under the assumption that [^{12}CO]/[^{13}CO] $\approx$ [^{12}C]/[^{13}C], namely τ[^{12}CO(1–0)]= 8–20 and 4–10 for [^{12}CO]/[^{13}CO] = 90 and 40, respectively. Thus, the observed ratios of ^{12}CO(2–1)/^{12}CO(1–0) and ^{12}CO(1–0)/^{13}CO(1–0) indicate that optically thick clouds dominate the molecular gas in the disk of M51.

A relatively larger R_{21} is observed in the outer disk (figure 10a). Some effects could yield a larger value. Since the CO(2–1) emission is optically thicker than the CO(1–0) emission [i.e., $\tau_{21} = 1.8\tau_{10}$ for T_{ex}(1–0)$\approx$ T_{ex}(2–1) $\approx$ 10 K and f(1–0)$\approx f$(2–1) from equation (8)], we see more deeply in molecular clouds in CO(1–0), and thus the assumption that both the emissions come from the same region of the clouds may not be correct, namely f(1–0) $< f$ (2–1). If there is a temperature gradient in the clouds, furthermore, the assumption that T_{ex}(1–0) $\approx T_{ex}$(2–1) may also not be satisfied. For instance, a molecular cloud heated from the outside by massive stars could yield T_{ex}(2–1) $> T_{ex}$(1–0) (e.g., Braine, Combes 1992; Gierens et al. 1992). These effects make R_{21} larger (equation 6). Alternatively, a larger R_{21} in the outer disk may be due to a smaller optical depth in the regions of the low CO intensity. Figure 10b shows the variation of R_{21} as a function of the integrated intensity of ^{12}CO(1–0). The ratio is $R_{21} = 1.05 \pm 0.38$ at $I_{CO} < 20$ K km s^{-1} while $R_{21} = 0.70 \pm 0.18$ at $I_{CO} > 20$ K km s^{-1}. A smaller I_{CO} of < 20 K km s^{-1} is observed mostly in the outer disk and interarm regions (figures 3b and 5). This can be explained if molecular clouds in the regions of low I_{CO} have a smaller optical depth due to the smaller column density. $R_{21} \approx 1$ corresponds to $\tau_{10} \approx 1$ for T_{ex}(1–0)$\approx T_{ex}$(2–1) $\approx$ 10 K and f(1–0)$\approx f$(2–1) which is much smaller than the typical τ_{10} ($\approx$ a few 10) of Galactic GMCs. Observations of the ^{13}CO/^{12}CO ratio would be very useful to confirm the effect in M51 that a smaller τ yields a larger R_{21}. It is unlikely that a larger R_{21} at $R > 120''$ is due to a higher excitation temperature, because the star-formation rate in these regions is low and the colour temperature of dust emission in the outer disk of M51 is not high (Smith 1982). The column density of hydrogen molecules corresponding to the critical I_{CO} = 20 K km s^{-1} is $N(H_2) = 4 \times 10^{21}$ H$_2$ cm^{-2} adopting the conversion factor of $N(H_2)/I_{CO} = 2 \times 10^{20}$ H$_2$ cm^{-2}, as estimated for the I_{CO} in M51 (Nakai, Kuno 1994).

The mean values of R_{21} previously measured in disks

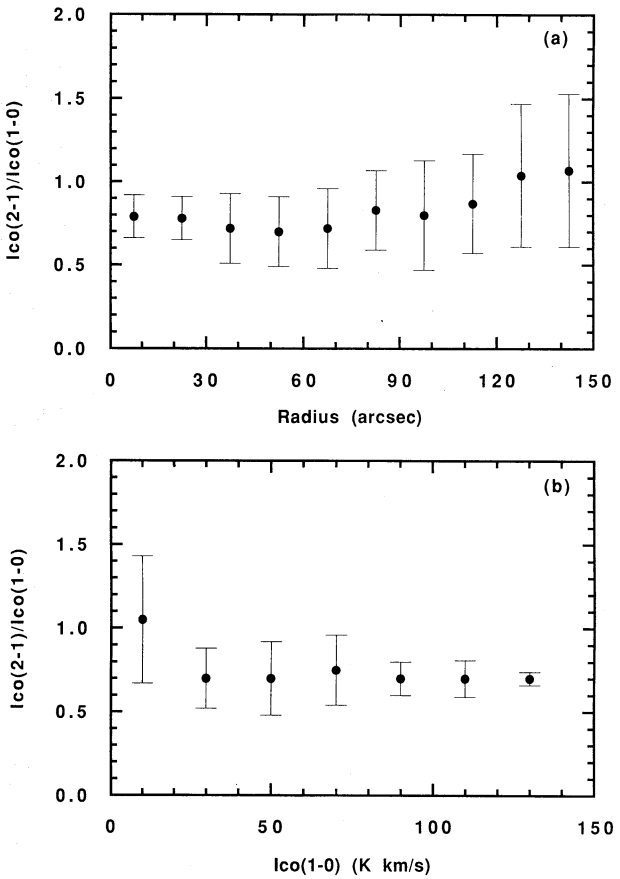

Fig. 10. (a) I_{CO}(2–1) to I_{CO}(1–0) ratio as a function of the distance from the center. If the line widths for J = 2–1 and J=1–0 are same, the I_{CO}(2–1)/I_{CO}(1–0) ratio corresponds to the T_{MB}(2–1)/T_{MB}(1–0) ratio. The error is 1σ. (b) Same ratio as a function of the CO integrated intensity.

Table 3. $^{12}CO(2–1)/^{12}CO(1–0)$ line intensity ratios of galaxies.

Galaxy	Type	Measured radius			$I_{CO}(2–1)/I_{CO}(1–0)^{\dagger}$	Reference
		arcsec	kpc	R/R_{25}^{*}		
M51	Sbc	150	7.0	0.45	0.80 ± 0.30	1
					0.8	2
NGC 891	Sb	270	12.4	0.86	0.75	3
NGC 2903	Sbc	65	2.4	0.19	0.70 ± 0.15	4
NGC 3628	Sb	60	2.0	0.18	0.80 ± 0.30	5
NGC 4414	Sc	50	2.3	0.49	0.68 ± 0.13	6
NGC 4736	Sab	80	2.4	0.24	0.7	7

* R_{25} is adopted from de Vaucouleurs et al. (1991).
† Mean value for the 6 galaxies is 0.74 ± 0.05 without incorporation of individual errors (1σ).
(1) This paper. Also 0.78 ± 0.27 at $R < 120''$ and 1.05 ± 0.43 at $120'' < R < 150''$, or 0.70 ± 0.18 at $I_{CO} > 20$ K km s^{-1} and 1.05 ± 0.38 at $I_{CO} < 20$ K km s^{-1} (2) Garcia-Burillo et al. 1993b. (3) Garcia-Burillo et al. 1992. (4) Calculated using the data of Jackson et al. (1991). (5) Calculated using the data of Boissé et al. (1987) and Reuter et al. (1991), assuming $\eta_{mb} = 0.49$ at 115 GHz in the observing year (1986) which was calculated from the aperture efficiency and the beam size quoted in Boissé et al. (1987). (6) Calculated using the data of Braine et al. (1993). (7) Gerin et al. (1991).

of galaxies are listed in table 3. All of the galaxies in the table show very similar values of $R_{21} \approx 0.7$–0.8, which is comparable to the above value in M51 and to the Galactic mean value of ≈ 0.8 (Sanders 1993). The data are, however, still too crude to derive a detailed variation of R_{21} with the galactocentric distance as well as with I_{CO}. Further observations of CO(1–0) and CO(2–1) with higher sensitivity, particularly for the low CO intensity, are required.

4. Summary

The $^{12}CO(1–0)$ emission from the optical disk of M51 has been mapped using the NRO 45-m telescope. The data are usable to obtain statistically meaningful results concerning the physical state of molecular gas, the features and dynamics of molecular arms, and their relation to star formation, in a typical spiral galaxy. Main results of CO distribution and molecular spiral arms are summarized as follows.

(1) Strong CO intensity concentrates in the central region (HWHM $\approx 40''$), showing a bar-like elongation with a semi-major axis of $\approx 25''$ and $P.A. \approx 110°$ along the stellar oval.

(2) The width of CO arm is FWHM $\approx$ 900–1000 pc, which is nearly constant with the distance from the center. Local maxima of the CO intensity are aligned along the arms with a nearly constant spacing of 1.6 ± 0.3 kpc.

(3) Both CO arms follow logarithmic spirals with a pitch angle of $21° \pm 5°$ at $40'' \leq R \leq 120''$, but are much disturbed at $R > 120''$ by a tidal interaction with a companion galaxy, NGC 5195.

(4) The CO arms are offset from the Hα arms by 440 pc $\pm$ 370 pc toward the inside, even at $R > 120''$, indicating that the outer disturbed arms as well as the inner arms are not material arms but are the patterns of the density wave.

(5) The $^{12}CO(2–1)/^{12}CO(1–0)$ ratio is constant to be 0.70 ± 0.18 at $I_{CO} > 20$ K km s^{-1} but larger (1.05 ± 0.38) at $I_{CO} < 20$ K km s^{-1}. The critical intensity of $I_{CO} \approx 20$ K km s^{-1} corresponds to $N(H_2) \approx 4 \times 10^{21}$ H_2 cm^{-2}. The mean ratio of 0.80 ± 0.30 over the whole disk is the same as those in disks of other normal spiral galaxies, including our Galaxy.

A detailed analysis of the relations with star formation and of molecular-gas dynamics will be presented in forthcoming papers.

We would like to thank the staff members of the Nobeyama Radio Observatory for encouragement to carry out this project.

References

Aaronson M., Mould J. 1983, ApJ 265, 1
Adler D.S., Lo K.Y., Wright M.C.H., Rydbeck G., Plante R.L., Allen R.J. 1992, ApJ 392, 497
Boissé P., Casoli F., Combes F. 1987, A&A 173, 229
Braine J., Combes F. 1992, A&A 264, 433
Braine J., Combes F., van Driel W. 1993, A&A 280, 451
Burbidge E.M., Burbidge G.R. 1964, ApJ 140, 1445
Byrd G.G., Haward S. 1990, in Dynamics and Interactions of Galaxies (Springer-Verlag, Berlin) p128
Cecil G. 1988, ApJ 329, 38
Cecil G., Rose J.A. 1984, ApJ 287, 131
Crane P.C., van der Hulst J.M. 1992, AJ 103, 1146
de Vaucouleurs G. 1979, ApJ 227, 729

de Vaucouleurs G., de Vaucouleurs A., Corwin H.G. Jr, Buta R.J., Paturel G., Fouqué P. 1991, Third Reference Catalogue of Bright Galaxies (Springer-Verlag, New York)
Ford H.C., Crane P.C., Jacoby G.H., Lawrie D.G., van der Hulst J.M. 1985, ApJ 293, 132
Garcia-Burillo S., Combes F., Gerin M. 1993a, A&A 274, 148
Garcia-Burillo S., Guélin M., Cernicharo J. 1993b, A&A 274, 123
Garcia-Burillo S., Guélin M., Cernicharo J., Dahlem M. 1992, A&A 266, 21
Gerin M., Casoli F., Combes F. 1991, A&A 251, 32
Gierens K.M., Stutzki J., Winnewisser G. 1992, A&A 259, 271
Goad J.W., Gallagher J.S. III. 1985, ApJ 297, 98
Goad J.W., de Veny J.B., Goad L.E. 1979, ApJS 39, 439
Hua C.T., Grundseth B., Nguyen-Trong T. 1987, Astrophys. Letters Commun. 25, 187
Jackson J.M., Eckart A., Cameron M., Wild W., Ho P.T.P., Pogge R.W., Harris A.I. 1991, ApJ 375, 105
Kaneko N., Morita K., Fukui Y., Sugitani K., Iwata T., Nakai N., Kaifu N., Liszt H.S. 1989, ApJ 337, 691
Kuno N., Nakai N., Handa T., Sofue Y. 1990, in Dynamics of Galaxies and their Moleculer Cloud Distribution, IAU Symp. No.146, ed F. Combes, F. Casoli (Kluwer Academic Publishers, Dordrecht) p77
Lester D.F., Harvey P.M., Joy M. 1986, ApJ 302, 280
Lo K.Y., Ball R., Masson C.R., Phillips T.G., Scott S., Woody D.P. 1987, ApJL 317, L63
Lord S.D., Young J.S. 1990, ApJ 356, 135
Makishima K., Ohashi T., Kondo H., Palumbo G.G.C., Trinchieri G. 1990, ApJ 365, 159
Nakai N., Kuno N. 1994, PASJ submitted
Nakai N., Kuno N., Handa T., Sofue Y. 1990, in Dynamics of Galaxies and their Moleculer Cloud Distribution, IAU Symp. No.146, ed F. Combes, F. Casoli (Kluwer Academic Publishers, Dordrecht) p63
Pierce M.J. 1986, AJ 92, 285
Rand R.J., Kulkarni S.R. 1990, ApJL 349, L43
Reuter H.-P., Krause M., Wielebinski R., Lesch H. 1991, A&A 248, 12
Rickard L.J., Blitz L. 1985, ApJL 292, L57
Rickard L.J., Palmer P. 1981, A&A 102, L13
Rose J.A., Cecil G. 1983, ApJ 266, 531
Rose J.A., Searle L. 1982, ApJ 253, 556
Rydbeck G., Hjalmarson Å., Rydbeck O.E.H. 1985, A&A 144, 282
Sandage A., Bedke J. 1988, Atlas of galaxies (NASA, Washington, D.C.)
Sandage A., Tammann G.A. 1974, ApJ 194, 559
Sandage A., Tammann G.A. 1975, ApJ 196, 313
Sandage A., Tammann G.A. 1981, A Revised Sharpley-Ames Catalog of Bright Galaxies (Carnegie Institution of Washington, Washington, D.C.)
Sanders, D.B. 1993, in Sky Surveys: Protostars to Protogalaxies, ASP Conference Series, Vol. 43, ed B.T. Soifer (Astronomical Society of the Pacific, San Francisco) p65
Scoville N., Young J.S. 1983, ApJ 265, 148
Smith J. 1982, ApJ 261, 463
Thronson H.A. Jr, Greenhouse M.A. 1988, ApJ 327, 671
Tilanus R.P.J., Allen R.J., van der Hulst J.M., Crane P.C., Kennicutt R.C. 1988, ApJ 330, 667
Toomre A. 1981, in The Large Scale Structure of The Universe, IAU Symp. No.79, ed M.S.Longair, J.Einasto (D. Reidel Publishing Company, Dordrech) p109
Toomre A., Toomre J. 1972, ApJ 178, 623
Tosaki T., Taniguchi Y., Kawabe R. 1994, ApJ submitted
Tully R.B. 1974a, ApJS 27, 415
Tully R.B. 1974b, ApJS 27, 437
Tully R.B. 1974c, ApJS 27, 449
van der Hulst J.M., Kennicutt R.C., Crane P.C., Rots A.H. 1988, A&A 195, 38
Verschuur G.L. 1993, AJ 106, 2580
Vogel S.N., Kulkarni S.R., Scoville N.Z. 1988, Nature 334, 402
Worden S.P. 1974, PASP 86, 92
Young J.S., Sanders D.B. 1986, ApJ 302, 680

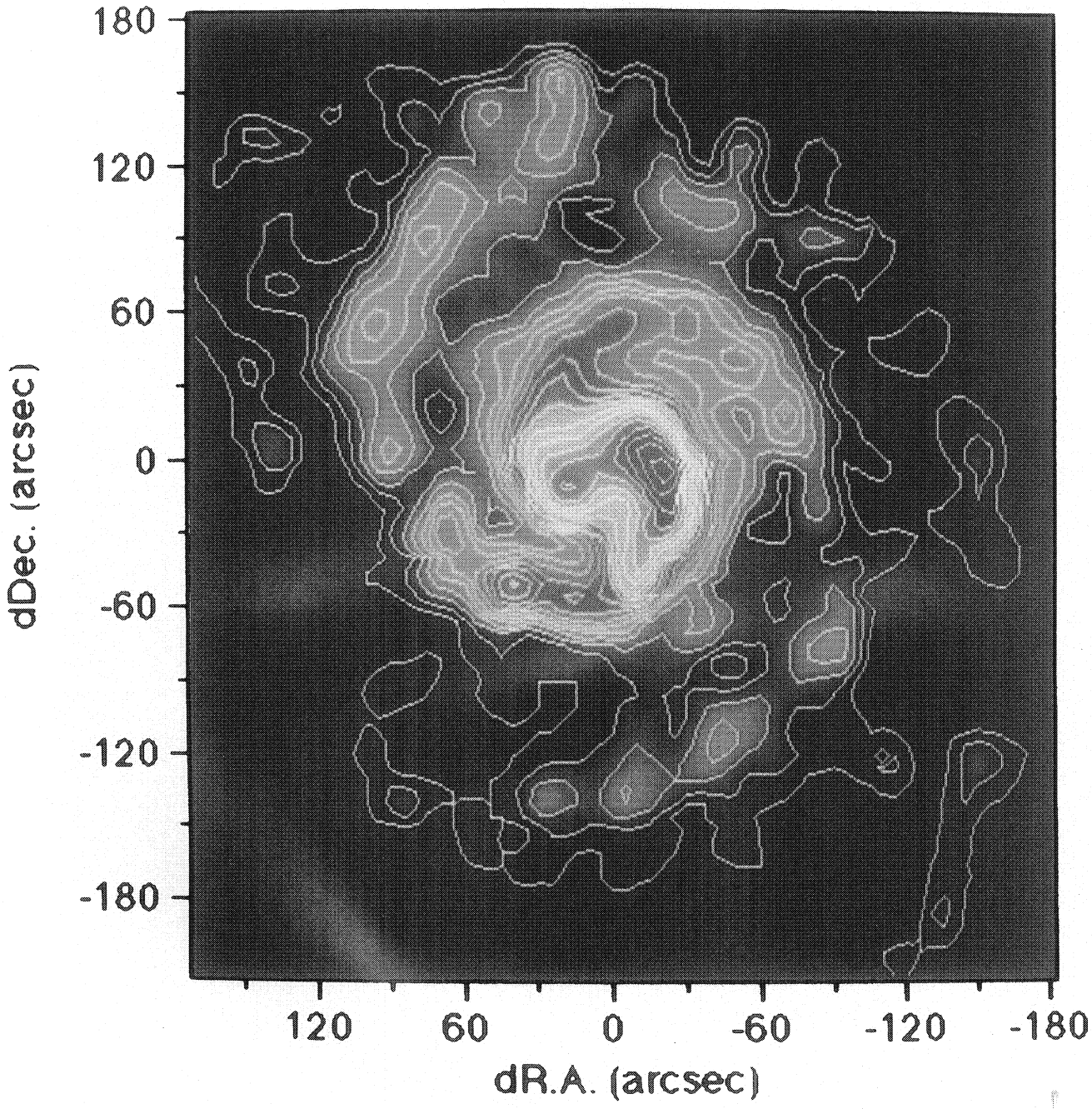

Fig. 6. Colour image of the CO integrated intensity of M51. Red represents strong intensity and blue weak intensity. The first contour and contour interval are 6 K km s^{-1}.

N. Nakai et al. (see Vol. **46**, 533)

Plate 17

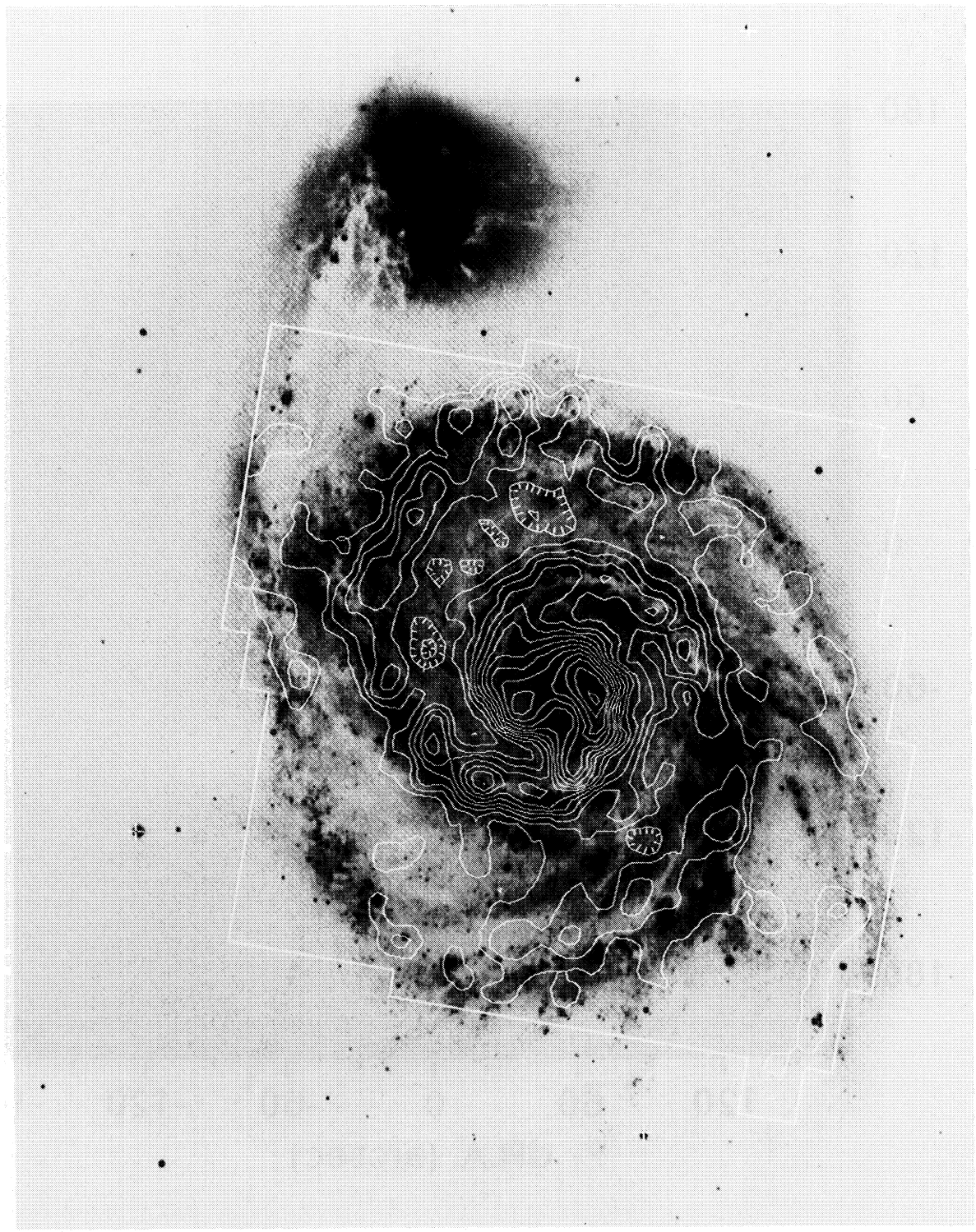

Fig. 8. Overlay of the contour map of the CO integrated intensity on an optical image (Sandage, Bedke 1988). The contour levels are same as figure 5. The top is north.

N. Nakai et al. (see Vol. **46,** 534)